Research Square

Preprints are preliminary reports that have not undergone peer review.
They should not be considered conclusive, used to inform clinical practice,
or referenced by the media as validated information.

Phenylalanine Gold Nanoclusters as Sensing Platform for π-π Interfering Molecules: A Case Study of Iodide

Amir Amiri-Sadeghan
Tabriz University of Medical Sciences
Tayebeh Zohrabi
Tarbiat Modares University
Ali Dinari
Gwangju Institute of Science and Technology
Reza Khodarahmi
Kermanshah University of Medical Sciences
Saman Hosseinkhani
Tarbiat Modares University
Soheila Mohammadi (Soheila.mohammadi@kums.ac.ir)
Kermanshah University of Medical Sciences

Research Article

Keywords: Phenylalanine, Gold nanoclusters, Fluorescent, π-π interaction, Iodide

Posted Date: September 22nd, 2021

DOI: https://doi.org/10.21203/rs.3.rs-908625/v1

License: This work is licensed under a Creative Commons Attribution 4.0 International License.
Read Full License

Abstract

The photo-physical properties of metal nano clusters are sensitive to their surrounding medium. Fluorescence enhancement, quenching, and changes in the emitted photon properties are usual events in the sensing applications using these nano materials. Combining this sensitivity with unique properties of self-assembled structures opens new opportunities for sensing applications. Here, we synthesized gold nanoclusters by utilizing phenylalanine amino acid as both capping and reducing molecule. Phenylalanine is able to self-assemble to rod-shaped nano structure in which the π-π interaction between the aromatic rings is a major stabilizing force. Any substance as iodide anion or molecule that is able to weaken this interaction influence the fluorescence of metal nano-clusters. Since the building blocks of the self-assembled structure are made through the reaction of gold ions and phenylalanine, the oxidized products and their effect of sensing features are explored.

1. Introduction

Metal nanoclusters (NCs) are the aggregates of few to tens of metal atoms either of a single or of multiple elements with the sizes smaller than 2 nm [1,2] which is a well-defined region of Fermi wavelength of an electron in conduction band. In this size regimen, the electron energy level changes from the quasi-continuous states to discrete ones [3–5]. Thermal conductivity, plasmon resonance and light reflection, all disappear, and molecule-like properties such as HOMO-LUMO transition, molecular chirality, intrinsic magnetism, and photoluminescence (PL) appear [4,6]. Due to their high surface energy, NCs are not stable in solution, and they must be protected by surface ligands. Many choices do exist as protecting ligands, from small molecules such as amines, phosphines, thiols [7], and amino acids to larger ones as polymers, and biomolecules [8] such as DNA [9–11], protein, and peptides [12,13]. These ligand-protected metal NCs not only offer high stability but also exhibit many physical and chemical properties that can be tailored based on their size and composition.

The photoluminescence [14] of NCs that is usually fluorescence is the most widely utilized feature of NCs in the sensing applications. Fluorescence decrease (turn off) [15] or enhancement (turn on) [16], blue [17] or red [18] shift of emission peak, resonance energy transfer (FRET) [19] are the possible responses to the presence of an analyte. The specificity of this type of NC-based sensors is governed by the specific interaction of the analyte with the metallic core or the protecting ligands. The analyte-metal core interaction based sensors are limited to few ones such as 1-fluorescence quenching of BSA-AuNCs with Hg^{2+} [20,21]. 2- Removing gold atoms from gold core of BSA-AuNCs by cyanide etching [22]. 3- Binding of silver ions to BSA-AuNCs [17]. On the other hand, ligand-analyte specific interaction is the cornerstone in many other sensing platforms that include many putative phenomenon as aggregation-caused quenching [23], aggregation induced emission [24], and ligand exchange [25]. The reason for such compatibility relies on the fact that the fluorescence of NCs is very sensitive to their local environment which is defined by the capping ligand and the medium. Among biomolecules, usually, DNA is an appropriate choice. Its flexibility can modulate the local environment of embedded or attached NC, and its

great potential as a recognition element (whether via base paring or acting as an aptamer) grants the specificity of the sensor. Since the consequences of the forces and bonds as hydrogen bonds are better-understood in the case of DNA, rational design and modifying sequence-dependent features are more facile comparing to other complex biomolecules such as peptides and proteins. However, on the other hand, self-assembled super molecules with simple building blocks are another class of biomolecules that may provide suitable sensing platforms. The limited number of involved forces for self-assembling make the outcomes more predictable. Therefore, combining the sensitivity of NCs fluorescence to their local environment with the capabilities of the stimuli-controlled morphology-transforming structures may open up new opportunities for sensing approaches. Previously, we have reported such a platform by utilizing phenylalanine dipeptide in combination with gold nanoclusters. The fluorescence of the gold NCs was sensitive only to the molecules that were able to disrupt the self-assembled structure [26]. Here, we have tested the same scenario with more simple and less costly building block of phenylalanine amino acid (Phe). In this study we have used iodide (I^-) or its oxidized form (I_2) as inorganic non-fluorescent substances capable of disrupting π-π stabilized assemblies [27]. On this way, the redox reaction of Phe and gold (III) ion was investigated to determine the oxidized species that build the sensor compartments. Finally, a specific simple sensing route for I^- is proposed.

2. Materials And Methods

2.1. Materials

All chemicals were of analytical grade and used as received.

2.2. Phenylalanine and gold reaction

UV-Vis absorbance of $HAuCl_4$ (1 mM) and Phe (1 mM) and the mixture of equal volumes of Phe and $HAuCl_4$ (2 mM each) were recorded by Thermo Fisher NanoDrop™ 2000 (Thermo Fisher, USA).

Phe, Phenylpyruvic acid (PhePyr) and phenylacetic acid (PheAc) were purchased from Titrachem, Iran. Working stocks of 100 mM were prepared by dissolving the Phe and PheAc in deionized water, and PhePyr in NaOH 1M. Testing the reduction capability of these compounds in various temperature and pHs were carried out for 30 minutes in 0.2 ml plastic vials by applying various temperatures in a dry bath incubator (Major science, USA). All pHs were recorded by pH indicator strips of McolorpHast (VWR, USA). The pHs were adjusted by adding NaOH or HCl with concentrations of 0.01 to 1 M.

To evaluate the proposed reduction mechanism for gold and Phe reaction, samples for Nessler's, and p-benzoquinone reactions were prepared as below: various molar ratios of Au:Phe of 0.5, 1, 2.5, and 3 were prepared by mixing Phe (20 µl, 100 mM) with adjusted volumes of $HAuCl_4$ solution which was neutralized to pH = 6 by adding NaOH. The final volumes of the reactions were set to 170 µl and heated at 60°C for four hours. Then, the precipitates were removed by centrifugations, and supernatants were examined by Nessler's, and p-benzoquinone reactions.

The ammonium production was examined by Nessler's reaction [28,29]. Nessler's reagent was prepared freshly by mixing NaOH (500 µl, 5M), KI (80 µl, 1 M), HgCl2 (100 µl, 100 mM) in the total volume of 1000 µl. The reaction was carried out at room temperature for 5 minutes by adding 2 µl of the samples into 20 µl of the Nessler's reagent. Various concentrations of samples of ammonium and Phe from 1.5 to 50 mM were tested to evaluate the reaction, and the absorbances were recorded at 420 nm.

The removal of amine from Phe was evaluated by p-benzoquinone [30]. The reagent was freshly prepared by mixing p-benzoquinone (100 µl, 100 mM in DMSO) and potassium phosphate buffer pH = 6.8 (900 µl, 1M). The reaction was carried out at room temperature for 30 minutes by mixing 50 µl of the reagent with 5 µl of the samples.

The second step of the reaction of gold with Phe and production of PhePyr and PheAc were confirmed by Fourier-transform infrared (FTIR) spectroscopy. The powders of Phe, PhePyr, and PheAc were dissolved in water, then heated at 60°C for four hours. The treated solutions and the samples from Phe-gold reaction were air-dried on glass slides at room temperature for a day, and mixed with KBr to form the pellets. FTIR spectra were recorded from 4000 (cm^{-1}) to 400 (cm^{-1}) by IR Prestige-21 (Shimadzu, Japan).

2.3. Optimizing the synthesis procedure

The effects of Au:Phe molar ratio, initial pH, and working buffer and pH on sensitivity of the synthesized Phe-Au NCs to iodide and its oxidized form were examined. The reaction mixtures were prepared by mixing Phe (500 µl, 100 mM) and $HAuCl_4$ (250 µl or 1200 µl, 100 mM), and initial pHs were adjusted to 6 or 7 by adding NaOH 1M. The final volume of the reactions was set to 1500 µl. The mixtures were heated at 60°C for four hours. Then, the clear supernatants were transferred to a new 10 ml vials after spinning down the precipitates, and diluted 10 times by deionized water. The fluorescence measurements were done in a 96-well black plate by Cytation^3 (BioTek, USA) by applying 100 µl of Phe-Au NCs in each well. Maximum excitation and emission wavelengths and fluorescence intensities were determined for all treatments. For evaluating the working pHs, the following buffers were prepared with 0.2 M concentration. Glycine-HCl (pHs = 2.2 and 3.6), Sodium citrate buffer (pHs 3.6, 4.4, and 5.6), sodium phosphate buffer (pHs 5.7, 6.7 and 8). The sensitivities to iodide ion, as a simple π-π modulating molecule, were determined by successively adding KI (100 mM) or its oxidized form by H_2O_2 in a 2 µl steps to each well containing 100 µl of 10x water-diluted Phe-AuNCs and 100 µl of prepared buffer. The calibration curves were estimated as the relation of F0/F to I^- concentration (mM) by Excel (2013) to evaluate the Stern-Volmer equation.

2.4. Synthesized Phe-AuNC features and its application

The Phe-AuNCs for characterization were prepared by Au:Phe molar ratio of 0.5. The reaction mixture contained Phe (500 µl, 100 mM) and $HAuCl_4$ (250 µl, 100 mM) in a 1.5 ml plastic vial and heat treated at 60°C in a dry bath for four hours.

Samples for transmission electron microscopy (TEM) analysis were prepared by placing 100X diluted drops of the as-prepared Phe-AuNCs on carbon-coated copper grids. The films on the TEM grids were allowed to stand for 10 min following which the extra solution was removed using a blotting paper and the grid allowed to dry prior to measurement. TEM measurements were performed on an instrument (Philips cm300, Japan) operated at an accelerating voltage of 200 kV.

Hydrodynamic diameter and zeta potentials were measured by dynamic light scattering (DLS) Malvern Nano ZS (Malvern, USA).

BSA-Au NC were synthesized as established by [31], and the fluorescence response of these BSA-AuNCs and Phe-AuNCs were compared respect to various molecules.

3. Results And Discussion

3.1. Phenylalanine and gold reaction

Phe as an amino acid carries amine and carboxyl groups which can act as chelating ligands to coordinate with metals such as Au (III) [32]. When Phe and $HAuCl_4$ are mixed, the ligand exchange takes place in a few minutes. The electronic transitions causing the absorption bands of $HAuCl_4$ in UV region (220 nm and 293 nm) are assigned to the ligand-to-metal charge transfer from *p* orbital of Cl to *d* of Au [33]. The absorbances related to these transitions are drastically decreased by adding Phe, indicating a ligand exchange (Fig. S1).

All 20 natural amino acids including Phe are able to reduce Au (III) ions to Au (0) in an appropriate pH and temperature [34,35], or by the aid of irradiation [36]. However, the empirically elucidated mechanisms are limited to few amino acids including glycine [37], alanine [38], tryptophan [39], and dopamine [40] (the decarboxylated derivative of 3,4 dihydroxyphenylalanine (L-DOPA)). In the case of tryptophan or L-DOPA, the functional groups of the side chains are responsible for the reduction. However, in the case of glycine and alanine the common features of amino acids, alpha amine and carboxyl moieties are involved in gold (III) reduction.

When a molecule is oxidized, electron is removed from the highest occupied molecular orbital (HOMO). Therefore, the oxidation potential of a molecule, as an indicator of its tendency to lose electron, is correlated with its HOMO energy level [35,41,42]. The calculated HOMO energies for alanine and Phe are similar, and the ionization of Phe is assigned to the joint contribution of the nitrogen lone pair and the π orbitals from the phenyl group [43]. On the other hand ,the electronic structure of Phe can be considered as the sum of benzene and alanine [44]. Therefore, the reaction pathway of gold reduction by alanine seems to be valid for Phe (Fig. 1). With valid assumption of this pathway, Phe can produce two atoms of gold in two steps. Phenyl pyruvate (PhePyr) and NH_4^+ are produced at the first step by removing the amine from Phe, and in the second step, PhePyr is oxidized to phenylacetatic acid (PheAc) by production of CO_2.

The proposed pathway was evaluated by the production of NH_4^+, removing of amine from Phe, and the production of PhePyr and PheAc. However, prior to evaluating the proposed pathway, the following five observations were taken into account to adjust the reaction condition tactfully.

First, the hydrothermal gold (III) reduction takes place at temperatures higher than 60°C and pH values ≥ 7 (Fig S2). Therefore, the synthesis reaction must be carried out in a temperature and pH range in which the hydrothermal reduction does not occur. This is important from stoichiometric point to make sure that all reduction electrons come from the reducing agent and not water.

Second, all pH values were adjusted by NaOH or HCl, and we avoided using any kind of buffer to adjust the pH of Phe and gold reaction. For example, phosphate buffer (PB) is usually mentioned as a non-involving buffer in gold reduction, however, we have observed that the reduction of gold happens in high concentrations of sodium PB. As depicted in Fig. S3, PB (1 M) could produce precipitates at temperatures from 40°C to 70°C and pHs of 5, 6, and 7. However, at pH = 8 no obvious particle formation was detected. In addition, by applying lower concentration of 0.1 M PB, the precipitates were observed only in pH = 5 and temperatures from 50°C to 70°C. This indicates the contribution of PB in complexation as well as the reduction of gold ions.

Third, the reduction by PhePyr is a fast reaction, and produces PheAc. As depicted in Fig S4, at room temperature, the reduction happens in pHs ≥ 7. As temperature rises, the reduction was observed in pHs ≤ 7 too. PhePyr is capable of reducing gold ions at pH = 6 and 7 at 60°C, and there is not any obstacle in front of the second step of the proposed pathway to proceed. The FTIR spectra of air-dried supernatant of the reaction production well-resembles PheAc.

Forth, as it is indicated in Fig. S5, PheAc does not go further oxidation, and hence, it is supposed to be the finial oxidized product especially if the pH of the reaction is adjusted below 7 (Fig. S4).

Fifth, unlike PhePyr, the reduction by Phe does not happen immediately at room temperature, and it roughly takes one to two days to produce visible particles. Hence, the activation energy for gaining electrons from amine seems to be greater than that from aldehyde (Fig. S6).

Taking these observations into account, the reaction mixture of Phe and $HAuCl_4$ was setup to be exempted from any additional buffering agents, and the pH value was adjusted to 6 by NaOH or HCl, and the reaction temperature was set to 60°C. In this condition, no thermal reduction takes place, and Phe and PhePyr are able to reduce gold ions while PheAc is not. As the reaction by PhePyr is faster than that by Phe, there is no kinetic bottleneck to cause PhePyr to accumulate. Therefore, it is expected that the final oxidized product is PheAc when the molar ratio of Au:Phe > 2. However, as it is going to be explained, proceeding the second step of the reduction reaction is determined by initial pH value.

In the first step of the reduction reaction, atomic gold and ammonium are produced through the conversion of Phe to PhePyr. The ammonium production was confirmed by Nessler's reaction. To assure that the other reagents as Phe and $HAuCl_4$ do not interfere with the detection of ammonium, their

interaction with Nessler's reagent were examined too. The reaction of Nessler's reagent with various concentrations of Phe, ammonium and $HAuCl_4$ are indicated in Fig. S7. As expected, Phe did not induce any color change, whilst ammonium generated a color shift from transparent to orange with a proper linear relation in the range of 1.5 to 50 mM. Nessler's reagent reduces $HAuCl_4$, and produces precipitates. These precipitates do not interfere with the detection of ammonium, because they can be easily removed by spinning down to leave the supernatant clear. As depicted in Fig. 2A, ammonium production was confirmed in all reactions of various molar ratios of Au:Phe (0.5, 1, 2.5, and 3). The evaluated ammonium concentrations were equal to the initial concentrations of Phe in the cases of Au:Phe = 2.5 and 3, showing the conversion of all amines of Phe to ammonium. Benzoquinone reacts with amine functional group selectively (Fig. S8). Figure 2B indicates the removal of amine from Phe in the reduction reaction. No amine was detected in the samples of Au:Phe = 2.5, and 3, showing that all Phe molecules have lost their amine group.

The second step of the reduction reaction is validated by FTIR spectroscopy by showing the production of PheAc. As Phe, PhePyr, and PheAc hold similar functional groups, we do not discuss the spectra in detail or try to assign the absorbances to specific molecular vibrational modes which are well-explained elsewhere [45–47]. Instead, we have used the similarity of the spectra as fingerprints to show the production of PheAc. Considering the stoichiometry of the proposed pathway, the final oxidized product must be totally PheAc when Au:Phe molar ratio is greater than two (here, 2.2). As shown in Fig. 3F, the spectra of Phe and gold reaction well-resembles PheAc when Au:Phe = 2.2 and initial pH is 7. This verifies the proposed pathway for reduction of gold ions by Phe.

Besides being the proof for the pathway, the obtained results by FTIR are notable especially for adjusting the reaction condition. As indicated in Fig. S9, the microscopic shapes of the air-dried Phe, PhePyr, and PheAc are very different that indicates the involvement of distinct molecular forces driving the self-assembling process. Different functional groups drive different combinations of hydrogen bonding which is an important force in the self-assembling process of similar molecules [48,49]. The building blocks of AuNC-carrying self-assembled structure as sensor are produced through the reduction reaction that may influence the features of the sensor.

When the molar ratio of Au:Phe is 0.5, the self-assembled structure is mainly composed of Phe (Fig. 3A&B). While, when Au:Phe > 2 and initial pH = 6, the second step of the reduction by PhePyr is restricted, and PhePyr accumulates (Fig. 3C&D). The accumulation of PhePyr shows that the second step of the reduction does not proceed to produce PheAc. As previously indicated (Fig S4), the reduction of gold ions by PhePyr is faster than that of Phe (Fig S4, S6), and the accumulation of PhePyr is not expected through a kinetic barrier. Also, the reduction of gold by PhePyr takes place at pHs ≥ 4 at 60°C (Fig. S4), and pH does not drop drastically to an unsuitable range when Phe and $HAuCl_4$ reacts. Moreover, the presence of PheAc in the reaction mixture of PhePyr and $HAuCl_4$ does not prevent reduction by PhePyr (data not shown). Hence, considering these observations the accumulation of PhePyr was not expected, and we could not explain it documentarily. A probable explanation may be that the pH

modulates the tendency of PhePyr to self-assemble or react further with $HAuCl_4$ which both are directed with its functional groups. Whatever the reason is, its consequence is important; The building blocks are totally made up of PhePyr in the case of Au:Phe > 2, and initial pH = 6. Also, extra gold ions remain in the solution due to an in-complete reaction. Increasing the fluorescence intensity of such a solution by adding $NaBH_4$ confirms the presence of extra gold ions (data not shown). On the other hand, when Au:Phe > 2, and initial pH = 7 the two steps of reduction reaction take place, and PheAc is produced (Fig. 3E&F), by which no fluorescent NC could form.

3.2. Optimizing the synthesis procedure

Since the application purpose of this study is to provide a sensing platform for π-π interacting molecules, the optimum synthesis route is the one with better sensing features. Here, iodide ion is selected as a simple non-organic and non-fluorescent π-π interacting substance.

The fluorescence and sensing features of as-synthesized AuNCs with different molar ratios of Au:Phe are summarized in Table S1. The maximum excitation and emission wavelengths were determined for all synthesis conditions. Similar excitation and emission wavelengths show that the formed AuNCs are similar in size or the number of atoms [6]. The synthesized NC in initial pH of 6 all showed similar maximum excitation and emission of 320/ 390 nm. But the maximum emission peak of the Au:Phe molar ratio of 0.5 with initial pH of 7 was 410 nm indicating a difference from those with initial pH of 6. The synthesis condition of Au:Phe = 2.2 and initial pH of 7 did not result in and fluorescence NCs showing that PheAc is not able to host or protect metal NCs.

The highest sensitives were obtained by Au:Phe molar ratios of 0.5 and working pHs of 5.6 and 6.7 in sodium PB. This shows that when the self-assembled NC-carrying structure is mainly composed of Phe (Au:Phe molar ratio = 0.5), the sensor is more sensitive than that when it is composed mainly of PhePyr (Au:Phe molar ratio = 2.2, initial pH = 6). Considering these observations, we selected the Au:Phe = 0.5 for further characterization.

3.3. Features of synthesized Phe-AuNCs and its characteristics as iodide sensor

The TEM images of the F-AuNCs are indicated in Fig. 4a, 4b which were analyzed by ImageJ software [50]. The sizes of self-assembled nanorods ofPhe are about 110×13 nm, and AuNCs are dark dots with average size of 1.8 ± 0.4 nm. The hydrodynamic diameter of 160 nm was obtained via the measurements by DLS that assumes a sphere shape for any particle (Fig. 4c). The isoelectric point of Phe-AuNCs is shown to be between 3 and 5 (Fig. 4d)

Here, we tested the fluorescence response of the Phe-AuNCs beside BSA-AuNCs to several molecules to evaluate some features of the sensing approach and if Phe-AuNCs can act as specific sensor for π-π interacting molecules like as Phe-Phe di peptide. Among these molecules Methylene blue, Azure B, Congo red, are evaluated as anti-amyloid substances that both prevent and disassemble the amyloid fibrils [51].

Iodine is proved to act to disassemble π-π stabilized molecules [27]. As indicated in Fig. 5a,b unlike BSA-AuNC the florescence of Phe-AuNC was not quenched by $HgCl_2$ showing that metallic core of NCs are not readily solvent available. Both BSA-AuNC and PheAuNC were sensitive to Methylene blue, Azure, Congo red but the sensitivity of Phe-AuNCs were higher to these molecules. SDS increased the fluorescence of Phe-AuNCs while reduced that of the BSA-AuNCs. Unlike BSA-AuNCs, Phe-AuNC was sensitive to iodide ions.The Stern-Volmer calibration curve in response to KI is indicate in Fig. 5c. The calculated LOD was 0.86 mM considering signal to noise reatio of three.

4. Conclusion

Here, we have shown that combining the features of a self-assembled structure with the sensitivity of metal nanoclusters to their local environment can lead to special sensing platform. Here, Phe as a simple building block of amyloid-like forming substrate in which the π-π stacking force holds a significant portion in the stability of the structure, is utilized in combination with gold NCs as stable non-reactive metal. On this way, the reduction reaction of Phe with $HAuCl_4$ is explored and is shown that Phe undergoes a twostep oxidation by which PhePyr and PheAc and an atom of gold are produced in each step. Moreover it is shown that by modulating the molar ratio and adjusting the reaction condition as pH and temperature the produced building blocks and hence the sensing feature can be managed. Phe-AuNCs are sensitive to the molecules that influence the π-π stabilized structure.

Declarations

Conflict of Interest

There are no conflicts of interest to declare.

Acknowledgements

This work was supported by grant from the Kermanshah University of Medical Sciences.

References

1. Chakraborty, I. & Pradeep, T. Atomically precise clusters of noble metals: emerging link between atoms and nanoparticles. *Chemical reviews*, **117**, 8208–8271 (2017).
2. Jin, R. Atomically precise metal nanoclusters: stable sizes and optical properties. *Nanoscale*, **7**, 1549–1565 (2015).
3. Kubo, R. Electronic properties of metallic fine particles. I. *Journal of the Physical Society of Japan*, **17**, 975–986 (1962).
4. Zheng, J., Nicovich, P. R. & Dickson, R. M. Highly fluorescent noble-metal quantum dots. *Annu. Rev. Phys. Chem*, **58**, 409–431 (2007).

5. Häkkinen, H. Electronic shell structures in bare and protected metal nanoclusters. *Advances in Physics: X*, **1**, 467–491 (2016).
6. Zheng, J., Zhang, C. & Dickson, R. M. Highly fluorescent, water-soluble, size-tunable gold quantum dots. *Phys. Rev. Lett*, **93**, 077402 (2004).
7. Jin, R. *et al.* Size focusing: a methodology for synthesizing atomically precise gold nanoclusters. *The Journal of Physical Chemistry Letters*, **1**, 2903–2910 (2010).
8. Wang, B. *et al.* Biomolecule Assisted Synthesis and Functionality of Metal Nanoclusters for Biological Sensing: A Review.*Materials Chemistry Frontiers*(2019).
9. Han, B. & Wang, E. DNA-templated fluorescent silver nanoclusters. *Analytical and bioanalytical chemistry*, **402**, 129–138 (2012).
10. Liu, J. DNA-stabilized, fluorescent, metal nanoclusters for biosensor development. *TrAC Trends in Analytical Chemistry*, **58**, 99–111 (2014).
11. Zhou, Z., Du, Y. & Dong, S. DNA–Ag nanoclusters as fluorescence probe for turn-on aptamer sensor of small molecules. *Biosensors and Bioelectronics*, **28**, 33–37 (2011).
12. Chevrier, D. M., Chatt, A. & Zhang, P. Properties and applications of protein-stabilized fluorescent gold nanoclusters: short review. *Journal of Nanophotonics*, **6**, 064504 (2012).
13. Hu, Y., Guo, W. & Wei, H. Protein-and Peptide-directed Approaches to Fluorescent Metal Nanoclusters. *Israel Journal of Chemistry*, **55**, 682–697 (2015).
14. Wilcoxon, J., Martin, J., Parsapour, F., Wiedenman, B. & Kelley, D. Photoluminescence from nanosize gold clusters. *The Journal of chemical physics*, **108**, 9137–9143 (1998).
15. Dadmehr, M., Hosseini, M., Hosseinkhani, S., Ganjali, M. R. & Sheikhnejad, R. Label free colorimetric and fluorimetric direct detection of methylated DNA based on silver nanoclusters for cancer early diagnosis. *Biosensors and Bioelectronics*, **73**, 108–113 (2015).
16. Sadeghan, A. A. *et al.* Fluorescence enhancement of silver nanocluster at intrastrand of a 12C-loop in presence of methylated region of sept 9 promoter. *Analytica chimica acta*, **1038**, 157–165 (2018).
17. Yue, Y., Liu, T. Y., Li, H. W., Liu, Z. & Wu, Y. Microwave-assisted synthesis of BSA-protected small gold nanoclusters and their fluorescence-enhanced sensing of silver (I) ions. *Nanoscale*, **4**, 2251–2254 (2012).
18. Li, B. *et al.* Aggregation-induced emission from gold nanoclusters for use as a luminescence-enhanced nanosensor to detect trace amounts of silver ions. *Journal of colloid and interface science*, **467**, 90–96 (2016).
19. Borghei, Y. S., Hosseini, M., Ganjali, M. R. & Hosseinkhani, S. A novel BRCA1 gene deletion detection in human breast carcinoma MCF-7 cells through FRET between quantum dots and silver nanoclusters. *Journal of pharmaceutical and biomedical analysis*, **152**, 81–88 (2018).
20. Xie, J., Zheng, Y. & Ying, J. Y. Highly selective and ultrasensitive detection of Hg2 + based on fluorescence quenching of Au nanoclusters by Hg2+–Au + interactions. *Chem. Commun*, **46**, 961–963 (2010).

21. Hu, D., Sheng, Z., Gong, P., Zhang, P. & Cai, L. Highly selective fluorescent sensors for Hg2 + based on bovine serum albumin-capped gold nanoclusters. *Analyst*, **135**, 1411–1416 (2010).
22. Liu, Y., Ai, K., Cheng, X., Huo, L. & Lu, L. Gold-nanocluster-based fluorescent sensors for highly sensitive and selective detection of cyanide in water. *Adv. Funct. Mater*, **20**, 951–956 (2010).
23. Goswami, N. *et al.* Copper quantum clusters in protein matrix: potential sensor of Pb2 + ion. *Analytical chemistry*, **83**, 9676–9680 (2011).
24. Yuvasri, G. S., Goswami, N. & Xie, J. *in Principles and Applications of Aggregation-Induced Emission*265–289(Springer, 2019).
25. Yuan, X. *et al.* Glutathione-protected silver nanoclusters as cysteine-selective fluorometric and colorimetric probe. *Analytical chemistry*, **85**, 1913–1919 (2013).
26. Zohrabi, T., Amiri-Sadeghan, A., Ganjali, M. R. & Hosseinkhani, S. Diphenylalanin nanofibers-inspired synthesis of fluorescent gold nanoclusters for screening of anti-amyloid drugs. *Methods Appl Fluoresc*, **8**, 045002 (2020).
27. Deng, Y. *et al.* Investigation of aggregation and assembly of alkali lignin using iodine as a probe., **12**, 1116–1125 (2011).
28. Leonard, R. H. Quantitative range of Nessler's reaction with ammonia. *Clinical chemistry*, **9**, 417–422 (1963).
29. Vanselow, A. Preparation of Nessler's reagent. *Industrial & Engineering Chemistry Analytical Edition*, **12**, 516–517 (1940).
30. Lorentz, K. & Flatter, B. Simplified colorimetry of α-amino nitrogen in plasma, serum, or urine. *Clinical chemistry*, **20**, 1553–1555 (1974).
31. Zhang, W. *et al.* One-step facile synthesis of fluorescent gold nanoclusters for rapid bio-imaging of cancer cells and small animals. *RSC Adv*, **5**, 63821–63826 (2015).
32. Glišić, B. Ä., Rychlewska, U. & Djuran, M. I. Reactions and structural characterization of gold (III) complexes with amino acids, peptides and proteins. *Dalton Trans*, **41**, 6887–6901 (2012).
33. Gangopadhayay, A. K. & Chakravorty, A. Charge transfer spectra of some gold (III) complexes. *The Journal of Chemical Physics*, **35**, 2206–2209 (1961).
34. Maruyama, T., Fujimoto, Y. & Maekawa, T. Synthesis of gold nanoparticles using various amino acids. *Journal of colloid and interface science*, **447**, 254–257 (2015).
35. Von Eschwege, K. G. & Conradie, J. Redox potentials of ligands and complexes-a DFT approach. *South African Journal of Chemistry*, **64**, 203–209 (2011).
36. Courrol, L. C. & de Matos, R. A. Synthesis of Gold Nanoparticles Using Amino Acids by Light Irradiation.*Catalytic Application of Nano-Gold Catalysts*,83(2016).
37. Chipman, A. *et al.* A computational mechanistic investigation into reduction of gold (III) complexes by amino acid glycine: a new variant for amine oxidation. *Chemistry–A European Journal*, **24**, 8361–8368 (2018).

38. Zou, J., Parkinson, J. A. & Sadler, P. J. Gold (III)-Induced Oxidation of Amino Acids and Malonic Acid: Reaction Pathways Studied by NMR Spectroscopy with Isotope Labelling. *Journal of the Chinese Chemical Society*, **49**, 499–504 (2002).
39. Selvakannan, P. *et al.* Water-dispersible tryptophan-protected gold nanoparticles prepared by the spontaneous reduction of aqueous chloroaurate ions by the amino acid. *Journal of colloid and interface science*, **269**, 97–102 (2004).
40. Du, S. *et al.* New insights into the formation mechanism of gold nanoparticles using dopamine as a reducing agent. *Journal of colloid and interface science*, **523**, 27–34 (2018).
41. Méndez-Hernández, D. D. *et al.* Simple and accurate correlation of experimental redox potentials and DFT-calculated HOMO/LUMO energies of polycyclic aromatic hydrocarbons. *Journal of molecular modeling*, **19**, 2845–2848 (2013).
42. Conradie, J. in *Journal of Physics: Conference Series.* 012045 (IOP Publishing).
43. Plekan, O., Feyer, V., Richter, R., Coreno, M. & Prince, K. C. Valence photoionization and photofragmentation of aromatic amino acids. *Mol. Phys*, **106**, 1143–1153 (2008).
44. Wang, F. & Ganesan, A. Fragment based electronic structural analysis of L-phenylalanine using calculated ionization spectroscopy and dual space analysis. *RSC Advances*, **4**, 60597–60608 (2014).
45. Barth, A. The infrared absorption of amino acid side chains. *Progress in biophysics and molecular biology*, **74**, 141–173 (2000).
46. Li, H. Q., Chen, A., Roscoe, S. G. & Lipkowski, J. Electrochemical and FTIR studies of L-phenylalanine adsorption at the Au (111) electrode. *Journal of Electroanalytical Chemistry*, **500**, 299–310 (2001).
47. Wolpert, M. & Hellwig, P. Infrared spectra and molar absorption coefficients of the 20 alpha amino acids in aqueous solutions in the spectral range from 1800 to 500 cm − 1. *Spectrochimica Acta Part A: Molecular and Biomolecular Spectroscopy*, **64**, 987–1001 (2006).
48. German, H. W., Uyaver, S. & Hansmann, U. H. Self-assembly of phenylalanine-based molecules. *The Journal of Physical Chemistry A*, **119**, 1609–1615 (2014).
49. Tamamis, P. *et al.* Self-assembly of phenylalanine oligopeptides: insights from experiments and simulations. *Biophysical journal*, **96**, 5020–5029 (2009).
50. Rueden, C. T. *et al.* ImageJ2: ImageJ for the next generation of scientific image data. *BMC bioinformatics*, **18**, 529 (2017).
51. Masuda, M. *et al.* Small molecule inhibitors of α-synuclein filament assembly., **45**, 6085–6094 (2006).

Figures

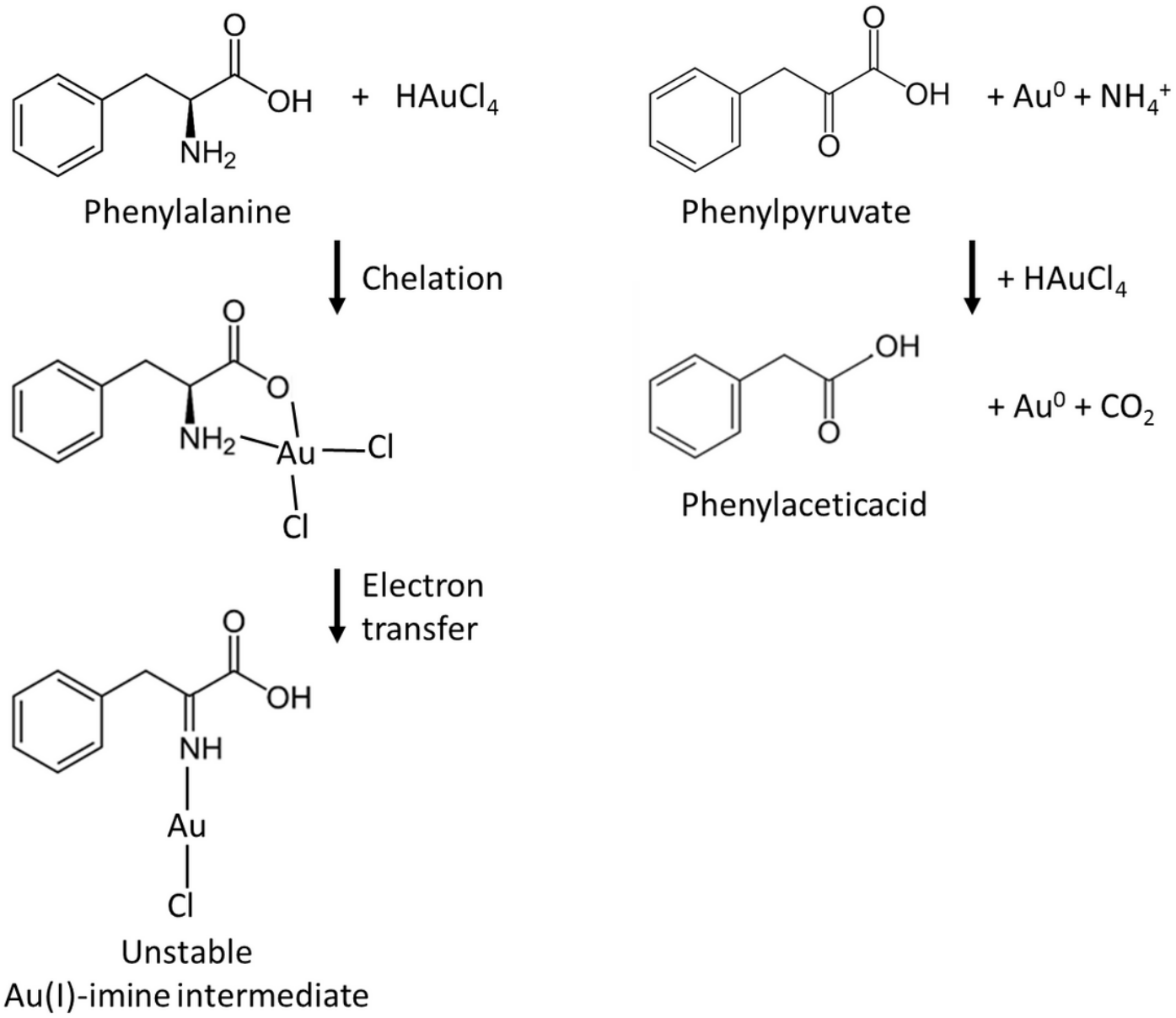

Figure 1

The proposed pathway of gold (III) reduction by phenylalanine

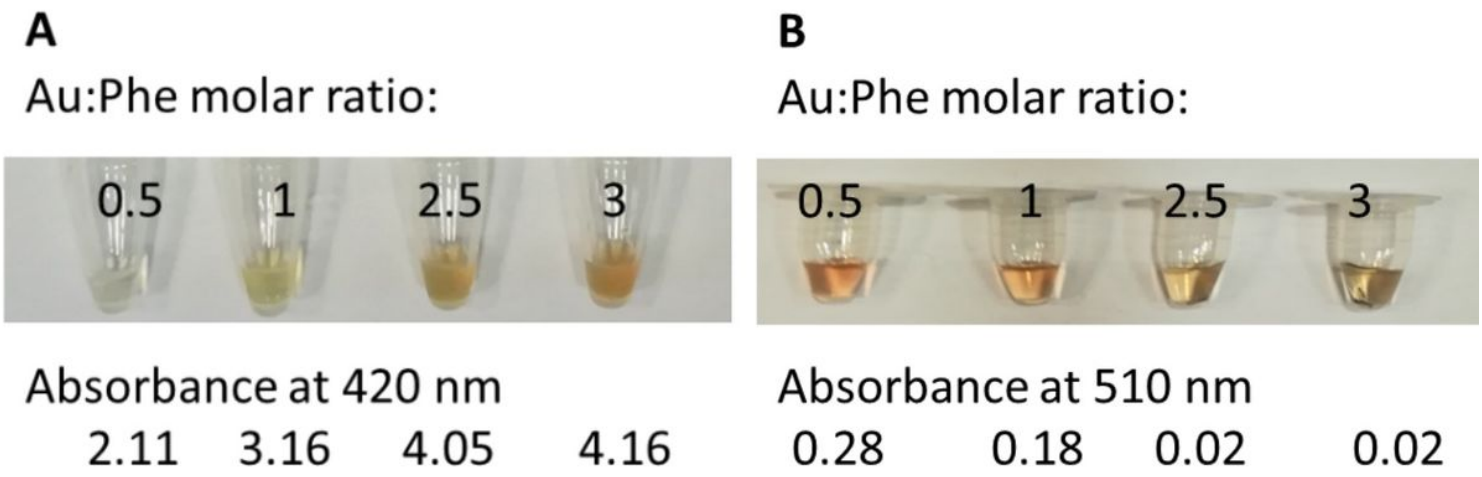

Figure 2

The first step of the reduction by amine of Phe. A: ammonium production is confirmed by Nessler's reaction. B: The removal of amine functional group from Phe is confirmed by benzoquinone reaction. There is no detectable amine at molar ratios of 2.5 and 3 while it still exists in lower molar ratios of 0.5 and 1.

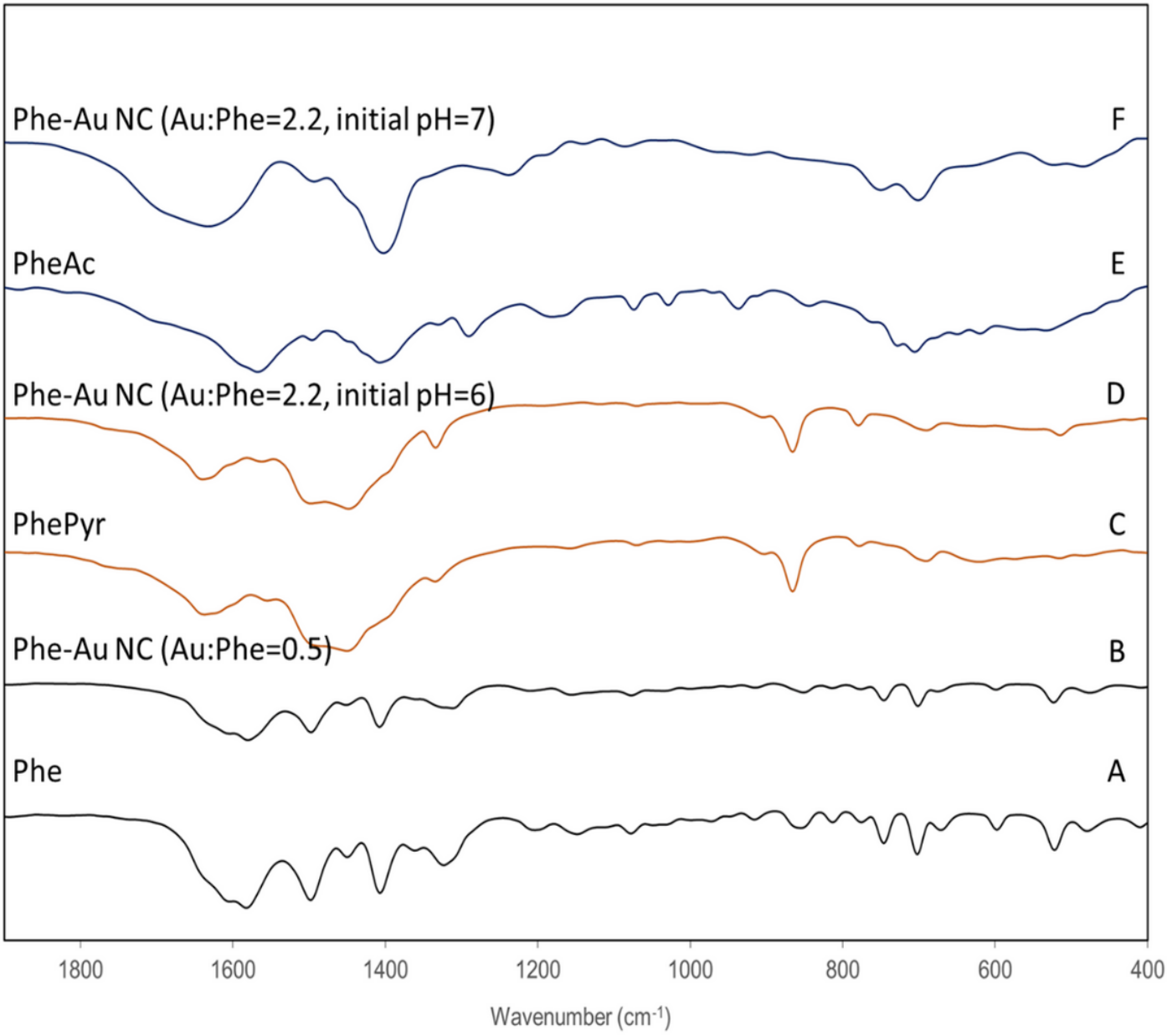

Figure 3

FTIR spectra of Phe, PhePyr, and PheAc that are similar to Phe-AuNCs when Au:Phe=0.5, Au:Phe=2.2-initial pH=6, and Au:Phe=2.2-initial pH=7 respectively, showing the production of PhePyr and PheAc.

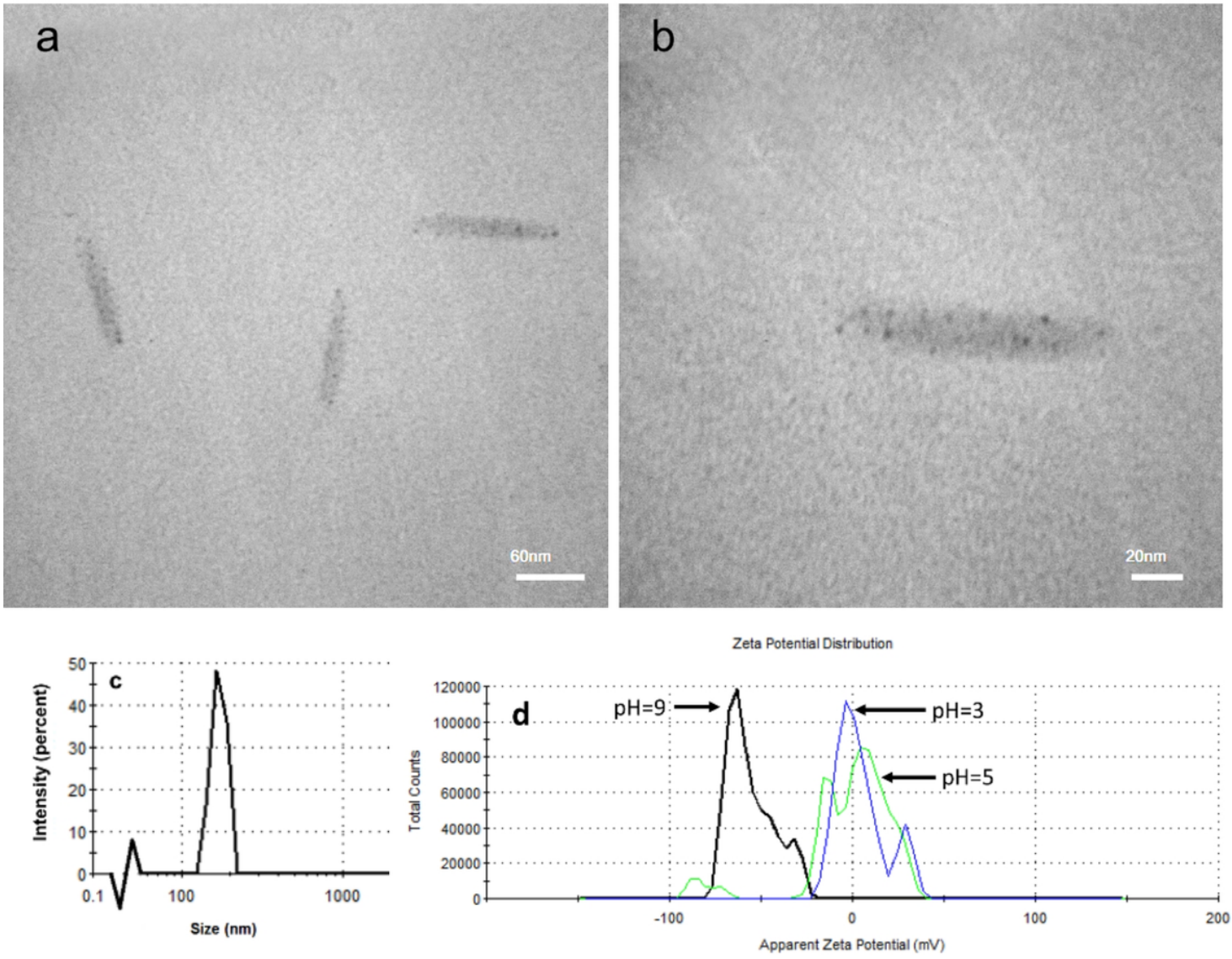

Figure 4

The features of Phe-AuNCs. a: TEM images of self-assembled nanorods of F-AuNCs; b: The dark dots on the nanorods with the sizes around 2 nm are assigned to metallic gold nanoclusters; c: Hydrodynamic size of the nanorods measured by DLS; d: the zeta potential of the nanorods at pH=9, 5, and 3

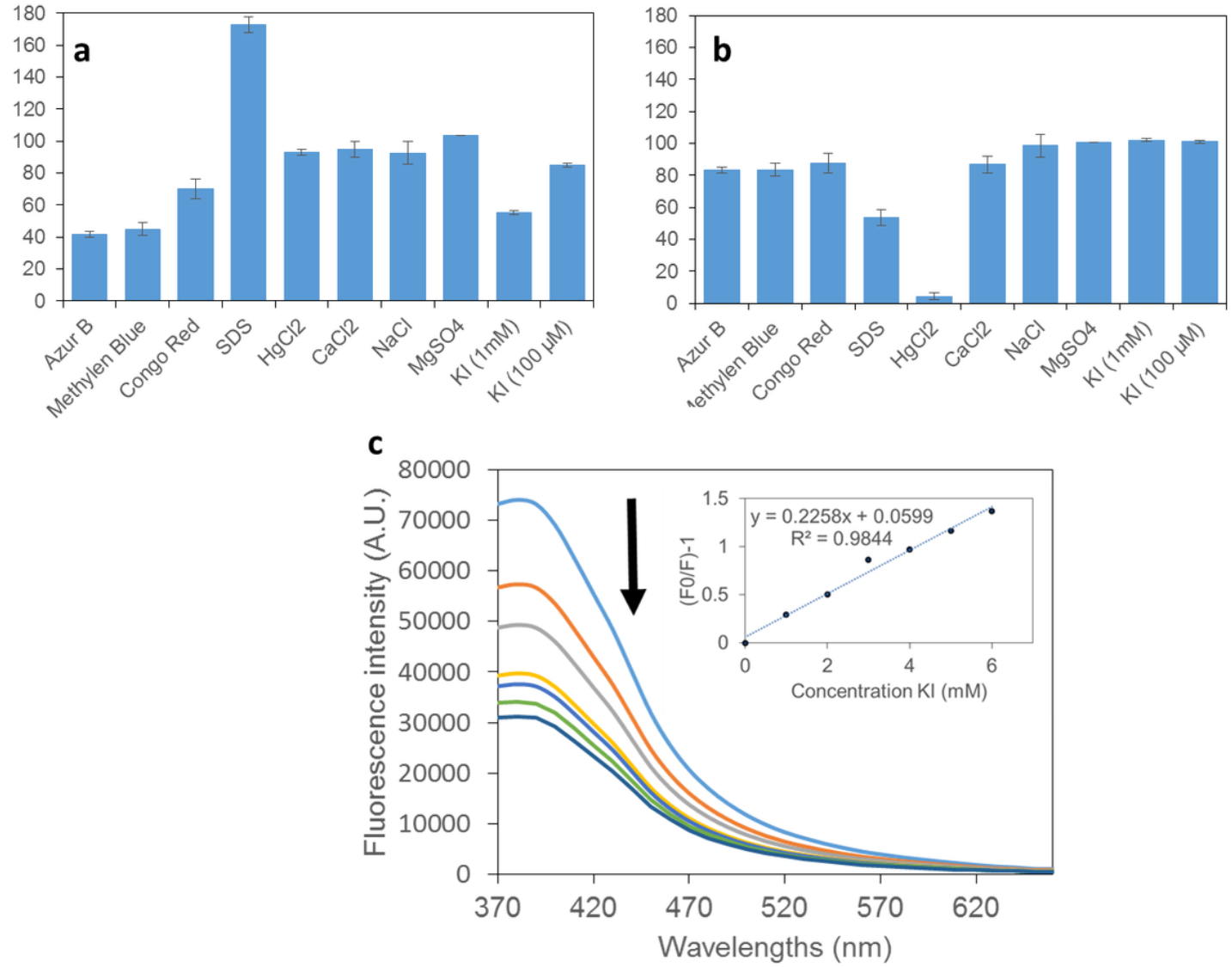

Figure 5

The fluorescence response of Phe-AuNCs (a), and BSA-AuNCs (b) to various substances, and the sensitivity of Phe-AuNC to KI.

Supplementary Files

This is a list of supplementary files associated with this preprint. Click to download.

- SuppPhenylalaninegoldnanoclusters.docx